Cancer Cell Invasion of Mammary Organoids with Basal-In Phenotype

*Eric Parigoris, Soojung Lee, David Mertz, Madeleine Turner, Amy Liu, Jason Sentosa, Sabra Djomehri, Hao Chen Chang, Kathryn Luker, Gary Luker, Celina G. Kleer, Shuichi Takayama**

Eric Parigoris, Dr. Soojung Lee, David Mertz, Madeleine Turner, Amy Liu, Jason Sentosa, Dr. Hao Chen Chang, and Prof. Shuichi Takayama
Wallace H. Coulter Department of Biomedical Engineering and The Parker H. Petit Institute of Bioengineering and Bioscience, Georgia Institute of Technology and Emory School of Medicine, Atlanta, GA 30332, USA
Email: takayama@gatech.edu

Dr. Sabra Djomehri and Prof. Celina G. Kleer
Department of Pathology and Rogel Cancer Center, University of Michigan Medical School, Ann Arbor, MI 48109, USA

Prof. Kathryn Luker and Prof. Gary Luker
Departments of Radiology and Microbiology and Immunology, University of Michigan Medical School and Department of Biomedical Engineering, University of Michigan College of Engineering, Ann Arbor, MI 48109, USA

Keywords: organoid, breast cancer, invasion, basal-in phenotype, basement membrane

Abstract

This paper describes mammary organoids with a basal-in phenotype where the basement membrane is located on the interior surface of the organoid. A key materials consideration to induce this basal-in phenotype is the use of a minimal gel scaffold that the epithelial cells self-assemble around and encapsulate. When MDA-MB-231 breast cancer cells are co-cultured with epithelial cells from day 0 under these conditions, cells self-organize into patterns with distinct cancer cell populations both inside and at the periphery of the epithelial organoid. In another type of experiment, the robust formation of the basement membrane on the epithelial organoid interior enables convenient studies of MDA-MB-231 invasion in a tumor progression-relevant direction relative to epithelial cell-basement membrane positioning. That is, the study of cancer invasion through the epithelium first, followed by the

basement membrane to the basal side, is realized in an experimentally convenient manner where the cancer cells are simply seeded on the outside of pre-formed organoids, and their invasion into the organoid is monitored. Interestingly, invasion was more prominent when tumor cells were added to day 7 organoids with less developed basement membranes compared to day 16 organoids with more defined ones.

1. Introduction

In vitro models of cancer are highly sought after as low-cost alternatives to investigate basic cell functions, such as proliferation and invasion, in addition to providing high-throughput platforms for drug-screening.[1] While a variety of platforms exist, ranging from Transwell migration assays to 3D microfluidic models, 3D spheroid/organoid cultures are of particular interest for their ability to be grown in co-cultures for long-durations of time if needed, used for high-throughput screens, and applied as patient surrogates for precision drug testing.[2,3] Organoids that mimic physiological cell heterogeneity, basement membrane structures, and 3D cellular organization are particularly valuable.[4]

Despite advances in the organoid field, there are a number of challenges for practical applications including lack of uniformity,[1,5] inconvenience of handling,[1] and difficulty of accessing the organoid lumen.[6] In ductal carcinoma *in situ* (DCIS), cancerous cells reside within the lumen of ducts on the side of the epithelium opposite the basement membrane. Accumulation of cells within this ductal lumen and loss of apicobasal polarity are both hallmark features of epithelial cancers that are commonly observed in both benign and invasive breast lesions.[7,8] In particular, the transition from noninvasive to invasive breast cancer is characterized by invasion out from the lumen of a breast duct – first through the epithelial cells, and then the basement membrane.[9]

Recently, we described a high-throughput, one-drop, one-organoid hanging drop culture platform that addresses the uniformity and convenience challenges of producing MCF10A cell mammary organoids. These cellular constructs are significantly larger (up to ~1 mm diameter) and have more complex cell organization compared to the conventional, small, Matrigel-embedded acini.[10] The term, organoid, is used here in the broader sense of 3D cellular structures that self-organize to recapitulate functional units of biological tissues.[10–12] Although created from a cell line, these large, self-organizing organoids exhibit multiple lineage phenotypes and cellular heterogeneity not observed in typical MCF10A acini.[10] Furthermore, unlike spheroids that have cell-filled interiors, this organotypic model has a large hollow interior and a sparse distribution of small cellular acini, reminiscent of terminal ductal lobular units (TDLUs). Here, we report on a minimal gel scaffold requirement to enable formation of these unexpectedly large organoids. We also reveal a surprising basal-in phenotype of the organoids where the basement membrane forms on the interior surface alongside an MCF10A epithelium. Importantly, this basal-in phenotype is stable and the basement membrane formed becomes more prominent over time. The basal-in phenotype and inner surface basement membrane formation by the MCF10A cells persist even when co-cultured with MBA-MD-231 breast cancer cells from day 0. When the MBA-MD-231 cells are added to the exterior of already formed MCF10A organoids, the tumor cells invade into the interior, although to a lesser extent at later time points when the basement membrane is more prominent.

While recent advances in breast cancer organoids derived from patients have been impressive,[4] the small lumens of cancer organoids and cell-filled spheroids make invasion studies difficult. Although there have been previous reports of 3D breast structures with

reversed polarity,[13–15] they typically represent acini which are on a smaller size scale, and the presence or location of the basement membrane is unclear. The large, basal-in phenotype mammary organoids and their breast cancer cell co-cultures described here, while currently still based on use of cell lines, are envisioned to open new opportunities for convenient, standardized, and physiological cancer cell invasion studies.

2. Results and Discussion

2.1 A Minimal Gel Scaffold is Key for MCF10A Organoid Formation

We recently described cellular self-assembly of unusually large mammary organoids in a hanging drop culture platform.[10] To better characterize the role of Matrigel from a materials perspective, we analyzed the gels that form under our experimental conditions in the absence of cells. It is noted that although Matrigel is known to form gels upon warming, the manufacturer's recommended concentration is 3 mg/mL and above, whereas the concentration used in our protocol is around 100 μg/mL, a concentration where gel formation is usually not expected. Indeed, when we follow the conventional protocol of mixing all media components (including Matrigel) at low temperature and then warming the media, gelling does not occur (**Supplementary Figure 1**). Gelling is minimal even when the Matrigel stock solution is directly added to pre-warmed media if fetal bovine serum (FBS) is absent. Interestingly, in our protocol where the concentrated Matrigel stock solution is added to pre-warmed media that also includes a high serum concentration, a gel-like substance develops. This gel-like substance is, initially, homogenously spread throughout the hanging drop (Supplementary Figure 1).

When MCF10A cells are present, the cells consolidate this gel-like substance (**Figure 1a-1c)**, as can be seen in Figure 1b where the arrow is pointing to the edge of the more localized

clear gel. Cell-assisted organization of a minimal Matrigel scaffold is evident when comparing the differences in gel organization with and without the addition of cells. Upon further incubation, the cells fully entrap the gel in the core of a 3D structure and are suggested to undergo coordinated rotational movement in order to maintain apicobasal polarity.[16] We found that the amount of Matrigel is important as both too little and too much Matrigel precludes formation of one large organoid in each drop. If no Matrigel is included in the culture, then the MCF10A 3D cultures form simple compacted spheroids instead of the much larger, hollow organotypic structures of interest in this paper (Figure 1d, 1e, and Supplementary Figure 1). Conversely, if too much Matrigel is included, the MCF10A cells form many small acinar structures, but never merge into one organoid. Even when the Matrigel concentration is appropriate (120 ± 10 μg/mL), if the media components are mixed when cold, following the manufacturer recommended protocol, the MCF10A cells form multiple small clumps, and often never completely merge into an organotypic structure (Figure 1f and 1g). Taken together, it is critical to add cold Matrigel to warm media with FBS to allow for pre-gelling, and the Matrigel concentration has been optimized to 120 ± 10 μg/mL.

2.2 The MCF10A Organoids have a Basal-In Phenotype

We further characterized the Matrigel in the organoid core at later timepoints. Using histological organoid sections as previously reported,[10] hematoxylin and eosin (H&E) staining (Figure 1h) revealed a network with pink hues inside of the organoid, suggesting presence of extracellular matrix proteins (ECM). A pan laminin-1,2 immunostain (Figure 1i) also showed extensive staining consistent with the notion that Matrigel (Corning, #356231), which is approximately 60% laminin (largely laminin-1), was encapsulated.

Laminin-5 has been used extensively as an indicator of the basement membrane for MCF10A cells grown in 3D culture, as it is known to be produced by the cells but is not present in significant amounts in Matrigel.[8,17–19] With MCF10A acini formed in conventional gel scaffolds or overlay systems,[8,16,17] the laminin-5 stains show a basal-out phenotype with the basement membrane on the outside of the small acinar structures (**Figure 2a**). Upon examination of laminin-5 staining of our organoids, however, we were surprised to discover the basement membrane to be on the interior surface of the organoid structure (Figure 2b). That is, at the outer periphery of the organoids, the distinct layer of laminin-5 (red) is on the inner side of the MCF10A cell nuclei (blue) (Figure 2c). We further assessed the organoids through integrin alpha-6 staining because of its established role in basement membrane adhesion.[20] Like the laminin-5 staining, the integrin alpha-6 was focused on the inner periphery of the organoid section, further supporting a basal-in cellular phenotype of these mammary organoids (Figure 2d).

We also analyzed the basement membrane organization of the acinar structures present in the interior of many organoids (Figure 2b). These smaller structures mostly maintain their basement membrane layer on the outside of the acini (Figure 2e), indicative of the more common basal-out polarity. Overall, Matrigel appears to play a critical role in the development of a basal-in phenotype. When it becomes entrapped inside of the organoid, the cells form around a Matrigel core (Figure 1a-1c). In turn, the organoid senses the basement membrane signal on the inside and the cells produce their own basement membrane, allowing for generation of the basal-in phenotype organoid structures.[14] On the other hand, the small acini in the organoid interior result in a basal-out polarity with an exterior basement membrane due to having Matrigel contact from the outside. These laminin-5 and integrin alpha-6 staining results reveal the intricacy of epithelial polarity within the organoid not

described in our prior publication with only cytokeratin 5/6 (CK 5/6) and cytokeratin 18 (CK 18) staining.[10] We therefore suggest that the basal-in phenotype is more complex than initially described.

The stable basal-in phenotype and prominent basement membrane observed in our large organoids stand in contrast to other reports of the smaller-sized, so-called inverted organoids where there is lack of characterization or presence of a stable basement membrane.[14] These smaller inverted organoids often show a mixture of inversion and non-inversion in the same organoid as revealed by various apical and basolateral markers, and the polarity flips back and forth between normal and inverted states quite readily.[6,21]

2.3 MCF10A Cells Form Organoids with a Basal-In Phenotype Even When Co-Cultured with MDA-MB-231 Cells from Day 0

We explored how co-cultures of MCF10A and MDA-MB-231 cells organize into different 3D structures under different culture conditions. Co-cultures of 3000 MCF10A and 300 MDA-MB-231 cells were performed in both the absence and presence of the minimal Matrigel scaffold at the time of seeding. We note that after the initial seeding, media exchange was performed with media that does not contain any Matrigel for all culture conditions tested. Organoids were tracked and imaged every few days for the 16-day growth period.

3D cultures without the minimal Matrigel scaffold resulted in a distinct separation between the two cell populations **(Figure 3a)**. The MCF10A cells formed a small compact spheroid, and the fluorescent MDA-MB-231 cells grew in loosely packed groups of cells surrounding

the MCF10A spheroid at random locations. These observations are similar to previously published co-cultures of MCF10A and MBA-MD-231 cells.[22,23]

Conversely, co-cultures with the minimal Matrigel scaffold exhibited a significantly different morphology. At day 2, there was a relatively well-mixed distribution of the two cell populations, although the overall size of the cellular structure was already significantly larger than co-cultures without Matrigel (p-value <0.000001). At later time points, the MDA-MB-231 cells organized into distinct patterns (Figure 3d) with one sub-population confined to the organoid interior, and another sub-population forming peripheral spheroids (indicated with a black arrow in Figure 3d). This 3D organization of MCF10A and MDA-MB-231 cells is robust and was reproduced among multiple independent co-culture experiments **(Supplementary Figure 2)**. In terms of morphology, the organoids seeded with Matrigel grew significantly larger compared to those seeded without Matrigel, although the discrepancy in area decreased over time in the culture. By day 16, the overall sizes were less different due to more extensive growth of the MDA-MB-231 cells in the condition without Matrigel (Figure 3b). In terms of roundness (Figure 3c), organoids without Matrigel experienced a statistically significant drop in roundness between days 7 and 10, largely because of the rapid growth of MDA-MB-231 cells at random peripheral positions. This also accounts for the higher standard deviations between different organoids for some days shown in Figure 3b and 3c. For organoids with Matrigel, the roundness stayed consistent throughout the culture; the small decrease is due to growth of small peripheral spheroids of MDA-MB-231 cells adjacent to the main organoid body. These differences between the two cell seeding conditions underline the importance of a minimal Matrigel scaffold at the time of seeding for producing the outside-in breast cancer organoids.

As seen in Figure 3d, the co-culture organoids often have a loosely attached peripheral spheroid of MDA-MB-231 cells adjacent to the main organoid structure while they are maintained in hanging drop culture. However, through harvesting and gentle pipetting, the peripheral spheroid is dissociated from the main body in a majority of the co-culture organoids. Figure 3 further shows H&E and laminin-5 images for one example where the peripheral spheroid remains attached to the organoid (e and f), and an example where the peripheral spheroid dissociated upon gentle pipetting (g and h). In both cases, the organoid maintained a basal-in phenotype, as can be seen by laminin-5 (red) predominantly localized on the inner side of the organoid epithelium. For the condition where the peripheral spheroid remained attached to the main organoid body, a microinvasion point with disorganization of the basement membrane is visible, reminiscent of initial stages of breast carcinoma *in situ*.[24,25] Overall, we show a robust and reproducible method for the long-term maintenance (20+ days) of co-cultures where the MCF10A cells show a basal-in phenotype.

MCF10A and MDA-MB-231 cells have been co-cultured previously, including in a 3D format as described by Carey *et al.* in 2013 **(Supplementary Figure 3)**. Interestingly, their experiments resulted in cell-filled spheroids with a core of MDA-MB-231 cells, followed by layers of MCF10A cells, and additional MDA-MB-231 cells on the periphery.[26] Our 3D co-cultures also formed structures with MDA-MB-231 in the core and in the periphery but within a much larger hollow organoid structure where the MCF10A cells form a thin epithelial shell with a distinct basement membrane (Supplementary Figure 3).[10]

At first glance, the two culture conditions are very similar, not only using the same cell types but also the same media, incorporation of Matrigel, and 3D culture. What could be the key difference leading to drastically different cellular organization outcomes? By testing different

MCF10A:MDA-MB-231 cell ratios from 1:1 to 1000:1, we excluded cell ratio as a major factor **(Supplementary Figure 4)**. The key difference is in whether the cell seeding conditions allow for minimal Matrigel scaffolding or not. Carey *et al.* performed cell seeding with media that only contains Methocel. The seeding media did not include Matrigel or 10% FBS, although Matrigel was introduced with the spheroid growth media following centrifugation and 2 hours of incubation. This is a condition that would not allow for cell-assisted Matrigel scaffolding as described in Figure 1a-1c.

For both experimental platforms, there are clear self-organizing behaviors likely due to cadherin mediated cell adhesion.[27,28] E-cadherin is expressed by the MCF10A cells and not the mesenchymal-like MDA-MB-231 cells, causing regions of mainly one cell type to form (**Figure 4b**). Our organoids follow similar, but slightly more distinct organization patterns, likely due to the initial Matrigel scaffolding and differences in time spent in culture. Carey *et al.* grew the spheroids for 48 hours and performed invasion experiments for 48 hours, but did not assess long-term viability. Because we grew the 3D co-cultures for 16-20 days, there is more time for growth of the overall structure, yielding larger cultures, in addition to more distinct cell separation. Carey *et al.* noted the presence of MDA-MB-231 cells at the periphery and core. We also initially see cells at the periphery and core; however, while the cancerous core remains intact, the cells initially at the periphery assemble and form a small ball adjacent to the main structure.

2.4 MCF10A Organoids as a Model to Study Ductal Carcinoma *In Situ*

One main advantage of the basal-in phenotype of the MCF10A organoids is direct access to the epithelial surface opposite the basement membrane, as the region in the media surrounding the organoid now represents the “luminal” side. In many previous organoid

models, access to the lumen is challenging, as time-consuming and technically demanding techniques, such as microinjection, are typically required.[6,29] To capitalize on this ease of "luminal" access in our model, we grew the MCF10A organoids to partial maturity (7 days) and placed 300 MDA-MB-231 cells in the media surrounding the organoid. The cancer cells were allowed to invade for 7-9 days before harvesting, fixing, and cryosectioning **(Figure 4a)**. Analysis revealed that the organoids generally maintain their epithelial integrity, as indicated by E-cadherin immunostaining (Figure 4b and **Supplementary Figure 5**). However, laminin-5 staining revealed disorganization of the basement membrane, as GFP labeled MDA-MB-231 cells could be observed inside a portion of the organoid sections that were analyzed (Supplementary Figure 5).

We further assessed how the timing of introduction of MDA-MB-231 cells affects penetration into the organoid. We chose day 7 and day 16 for introduction, and allowed the cells to invade for 9 days (thus, cultured to days 16 and 25, respectively). In these experiments, the MCF10A cells were stably transduced with RFP to contrast with the green fluorescent MDA-MB-231 cells. Furthermore, invasion was analyzed using confocal stacks obtained after optical clearing of the organoids (Figure 4c and **Supplementary Figure 6**). When cancer cells are introduced to day 7 MCF10A organoids, a majority of organoids were invaded, whereas only a small fraction of day 16 organoids experienced MDA-MB-231 invasion (Figure 4f). Importantly, this trend correlates with prominence of the basement membrane – initially, it is largely disorganized, has weaker laminin-5 staining, and is highly discontinuous along the inner periphery of the organoid structure (Figure 4d**)**. However, by day 16, the basement membrane is much more pronounced, with a prominent band along the basal side of the MCF10A epithelium (Figure 4e).

Because of the ease of use and high-throughput nature of this platform, there are significant biological applications. For example, we envision that our system will be useful for the study of the early invasion steps in DCIS-to-invasive carcinoma progression. DCIS is a type of non-invasive breast cancer that accounts for approximately 25% of all breast carcinoma diagnoses.[30] It has been demonstrated that approximately 30% of untreated cases of DCIS develop IDC within 10 years.[31] At present, there are no biomarkers that can predict which cases of DCIS will progress to invasion.[25,31] Therefore, there is currently a need for a better understanding of underlying factors responsible for the disease progression and for the development of prognostic biomarkers.

To help study disease progression, a few 2D and 3D models of DCIS have been developed ranging from co-culture spheroid models[9,30] to microfluidic devices[31–34] that recapitulate the key physiological features of the disease and serve as potential platforms for assessment of invasion and transition into IDC. One model of interest is the work done by Sameni *et al.* that details the use of mammary architecture and microenvironment engineering (MAME) to produce 3D models of DCIS invasion.[9,35] While this model allows for the study of basement membrane breach and invasion, the system is gel-embedded, the cells form small acini, and luminal access is highly limited. On the contrary, microfluidic devices can facilitate investigation of environmental factors of cancer invasion over long periods of time. Previously, Choi *et al.* developed a microfluidic platform consisting of upper and lower channels to mimic the ductal lumen and vascular layer, respectively. In between the two channels, a DCIS spheroid was placed on a mammary epithelium layer grown on a Matrigel-coated vitrified collagen membrane, which additionally covered a stromal layer consisting of cancer-associated fibroblasts (CAFs).[33] Another microfluidic platform by Bischel *et al.* takes advantage of viscous finger patterning to create a hollow lumen lined with MCF10A cells,

which can be filled with MCF10DCIS.com cells to mimic the disease state. To further increase physiological relevance, the chip contains two side channels, which can be filled with mammary fibroblasts.[31] While versatile, microfluidic models are structurally complex and have lower throughput.

In addition to models specific to the study of DCIS, there are several alternative *in vitro* and *in vivo* models of breast cancer invasion. While Transwell models are simple and effective to use, they do not encapsulate the cancer microenvironment and can only assess single cell motility. Optimized cancer invasion models also exist, such as the Chemicon/QCM ECMatrix Cell Invasion Assay which measures invasion by post-labelling with fluorescent dye. However, it is only an endpoint assay,[36] and it further does not provide a true cell-produced basement membrane, but rather an exogenous extracellular matrix layer. *In vivo* invasion assays take advantage of animal basement membranes, such as sea urchin embryo basement membrane (SU-ECM) and chick embryo chorioallantoic membrane (CAM), for more accurate modeling of complex systems.[37,38] Despite the ease of use of these assays, their animal-origin limits availability of reagents and the differences in drug metabolism with mammals make drug testing difficult.[38]

We propose hanging drop organoids that possess MCF10A cell-produced, native basement membranes as a platform for studying cancer cell invasion. Our model's basal-in phenotype allows it to serve as a convenient platform for the study of invasive abilities of breast cancer cells where the "luminal" epithelium on the side opposite the basement membrane is readily accessible from the organoid exterior. Organotypic models that assess invasion in a manner similar to DCIS progression to IDC can pose a challenge for throughput and feasibility if the basement membrane is located on the outside layer, as microinjection into the lumen would

be required, and invasion outwards would be assessed. The results in Figure 4 demonstrate the potential of our basal-in phenotype organoid, as we have shown successful invasion of triple negative breast cancer cells from the "luminal" side of the epithelium (represented by the media surrounding the organoid), through the basement membrane, to the basolateral side of the epithelium (represented by the inside of the organoid). Cancer cells can be pipetted into the surrounding microenvironment of the organoid, and invasion inwards can be assessed through histology and microscopy. With our current platform, typically 192 organoids (every other well of a 384-well plate) can be simultaneously assayed per plate and maintained in culture for 25+ days.

Limitations of the current platform include the use of cell lines rather than primary cells, only mammary epithelial cells and tumor cells, and low-throughput tissue sectioning and clearing methods for much of the analysis. As DCIS transitions to IDC, there is a well characterized and progressive loss of the myoepithelium along with its associated differentiation markers; *in vivo*, these cells are responsible for basement membrane deposition.[24,39] As such, the presence or absence of these two layers, in most cases, is used to differentiate between DCIS, DCIS suggestive of invasion, or IDC.[40–42] Because our model does not contain a deliberately seeded population of myoepithelial cells, this is one aspect that limits its physiological relevance to the bilayered epithelium found in many types of DCIS. Additionally, although our hanging drop platform is a high-throughput technique, the plates can be difficult to handle because of risk of droplet loss due to bumping, rapid evaporation when left in the open, and difficulty of programming automatic imaging platforms to focus on cells inside hanging droplets. The methods and concepts, however, should be readily expandable to test for use of primary cells, incorporation of additional cell types, and use in mechanistic assays.

3. Conclusion

Building off of our previously described mammary organoid platform,[10] we newly discovered that these organoids have a basal-in phenotype. Laminin-5, an indicator of the basement membrane, is located on the interior surface of the organoid structure consistently across all samples that were imaged. We found that cell-assisted scaffolding through the reorganization of Matrigel and entrapment in the organoid core plays a critical role in this basal-in phenotype. While several reports of so-called inverted organoids exist,[6,21,43,44] prior systems observe much smaller acinar structures that often have mixed polarity, undergo easy inversion and re-inversion based on culture environment change, and have unclear basement membrane presence. In contrast, our experiments consistently produce organoids that are large and have a well-developed laminin-5-rich basement membrane with a basal-in orientation. Importantly, our organoids maintain their basal-in phenotype even when co-cultured with MDA-MB-231 cells from initial seeding, though sometimes there is disorganization in the basement membrane with sub-populations of MDA-MB-231 cells located both inside and outside of the organoid. Capitalizing on the robust basal-in phenotype of the MCF10A organoids, we propose that our model will be useful to study the early steps of breast carcinoma invasion as it occurs in DCIS-to-invasive carcinoma progression. The robust maintenance of the basal-in phenotype also allows for long-term studies of at least 25 days. While the specific cellular model described focuses on mammary tissues and breast cancer, the methods and concepts, such as cell-assisted Matrigel scaffolding for robust production of large organoids with a basal-in phenotype, may be applicable to a broad range of organ, tissue, and cancer types. This is particularly relevant, given the previously reported potential for polarity inversion of organoids and acini formed by epithelial cells from the breast,[13–15] kidney,[21,43,44] gut,[6,45] and lung.[43]

4. Experimental Section

2D cell culture: MCF10A cells were purchased from ATCC and cultured in DMEM/F12 (Gibco) supplemented with 5% horse serum (Gibco), 20 ng/ml heparin-binding epidermal growth factor (HB-EGF) (Peprotech), 0.5 μg/ml hydrocortisone (Sigma), 100 ng/ml Cholera toxin (Sigma), 10 μg/ml insulin (Sigma), and 1% penicillin/streptomycin (pen/strep) (Gibco).[8] MDA-MB-231 stably transduced with GFP[46] were grown in DMEM (Gibco) supplemented with 10% fetal bovine serum (FBS) (Gemini), 1% pen/strep, and 1% GlutaMAX (Gibco). Cultures were maintained at 37 °C and 5% CO_2 in T75 culture flasks. Cells in 2D culture were routinely passaged at 70-80% confluence.

MCF10A RFP transduction: MCF10A cells were seeded at a density of 100,000 per well in a 6-well tissue culture plate. After allowing cells to attach overnight, media was aspirated and cells were rinsed with PBS. Then, 2 mL of transduction media containing heat-inactivated horse serum, polybrene at a final concentration of 5 μg/mL (Sigma #107689), and RFP lentivirus (Cellomics Technology) at a final concentration of 400,000 TU/mL for a total multiplicity of infection (MOI) of 8 was added to the cells. Transduction occurred for 8.5 hours, after which the transduction media was aspirated and the cells were rinsed with sterile PBS. Then 2 mL of fresh media was added to the cells. The cells were expanded and the RFP-hi positive population was selected for using florescence-activated cell sorting (FACS). Before seeding into organoids, the cells were maintained in growth media containing 1 μg/mL puromycin to maintain selective pressure against unlabeled cells.

3D organoid culture: To grow MCF10A mammary organoids in hanging drop culture, previously described custom plates[47] were soaked overnight in 0.1% F108 pluronic solution (Sigma 542342), rinsed with water, and UV sterilized for 20 minutes on each side with a

UVP Crosslinker (Analytik Jena). To minimize evaporation of the drops, the plate was sandwiched between a 96-well round bottom plate, and the wells filled with distilled water. To provide further humidity, the troughs of the hanging drop plate were filled with distilled water and sterile gauze pads. Organoids were seeded and maintained in hanging drop culture as previously described[10]. Briefly, 3000 MCF10A cells were seeded in every other well of a 384-well hanging drop plate in a final volume of 25 µL. The cells were supplemented with 0.24% Methocel (A4M, Sigma), 1.5% Matrigel (Corning, #356231 Growth Factor Reduced Basement Membrane Matrix), and 10% FBS to promote initial aggregation, growth, and subsequent hollowing[10,48]. To ensure the organoids exhibited a basal-in phenotype, cold Matrigel was added to pre-warmed growth media containing FBS and Methocel prior to introducing the cells. On day 3 of organoid culture, the media was exchanged 3 times to wash out the seeding supplements using a CyBio FeliX liquid handling machine (Analytik Jena). To exchange media, 9 µL was removed, and 10 µL was added to account for evaporation. For routine culture, media was exchanged 2 times every 2-3 days. Organoids were maintained in culture for 16 to 25 days. For co-culture experiments, 300 MDA-MB-231 cells were seeded with 3000 MCF10A cells. Cells were seeded in the same media as the MCF10A mono-culture organoid seeding media containing 1.5% Matrigel, 10% FBS, and 0.24% Methocel in complete MCF10A growth media. During routine media changes, complete MCF10A growth media was also used to replenish the hanging drops following the exchange protocol described above.

Cancer invasion experiments: MCF10A organoids were seeded as described using 3000 cells, and grown in culture for 7 or 16 days. On day 7 or day 16 of culture, 300 MDA-MB-231 cells were introduced into each drop, and the cultures were maintained for an additional 7-9 days.

At the end of the experimental timepoint, the organoids were harvested, fixed, and prepared for cryohistology or optical clearing.

Organoid imaging and morphology analysis: While organoids were maintained in hanging drop culture, they were imaged every 2-3 days using an EVOS FL Auto 2 microscope (Thermo Fisher) with a 4x objective. For basic morphology analysis, Image J was utilized.[49] The images were converted to binary, inverted, and the "Analyze Particles" macro was used to calculate both the area and roundness/circularity of the organoids.

Sample embedding and cryosectioning: Organoids were harvested from the hanging drop plate upon completion of the experiment, and washed 3 times in PBS. Samples were fixed in 4% paraformaldehyde (Alfa Aesar) for 1 hour at room temperature and washed with PBS. To aid in the visualization of the organoids, they were stained with 0.5% methylene blue (Ricca Chemical Company) for 10 minutes, followed by several PBS washes to remove the excess dye. A small amount of optimal cutting temperature (OCT) (Tissue-Tek) was added to a cryomold, and approximately 15 organoids were added to each mold. Subsequently, the organoids were covered with additional OCT. Isopentane (Sigma) was cooled in liquid nitrogen, and samples were flash frozen in the isopentane for less than 2 minutes. Cryoblocks were stored at -80 °C, and 10 μm sections of the organoids were obtained using a CryoStar NX70 cryostat (Thermo Fisher).

H&E staining and microscopy: Mounted sections were stored at -20 °C and thawed for 5 minutes prior to H&E staining. An ST5010 Autostainer XL (Leica) was used to perform the H&E staining. Samples were coverslipped with Xylene and Cytoseal 60 (Richard-Allan

Scientific). The samples were imaged using a DMi1inverted microscope equipped with a color camera and 10x objective (Leica).

Immunofluorescence staining and microscopy: Mounted sections were rinsed with PBS and permeabilized with 0.2% Triton X-100 (Sigma) for 5 minutes. The sections were washed 3 times with PBS and blocked with 4% bovine serum albumin solution (BSA, Millipore Sigma, #82-067) for 1 hour at room temperature. Rabbit anti-E-cadherin (Cell signaling #3195, 1:200 dilution), Rabbit anti-laminin-1,2 (Thermo Fisher #PA1-16730, 1:1000 dilution), Rabbit anti-laminin 5 (Abcam #ab14509, 1:200 dilution), and Rabbit anti-integrin alpha-6 (Thermo Fisher # 27189-1-AP, 1:500 dilution) primary antibodies were added to the samples, and incubated at 4 °C overnight. Primary antibodies were then removed, and samples were washed 3 times with 1% BSA solution in PBS. Secondary antibodies were incubated with the samples for 2 hours at room temperature. For all stains, Goat anti-Rabbit Alexa Fluor 594 was utilized as the secondary antibody (Invitrogen #A11012, 1:1000 dilution). Slides were rinsed 3 times with PBS, and incubated with DAPI (Thermo Fisher, 1.4 μM) for 15 minutes at room temperature. The slides were rinsed 3 times with PBS, briefly dried, and mounted using ProLong Diamond Antifade mounting media (Thermo Fisher #P36965). A DMi8 inverted epifluorescence microscope (Leica) equipped with 10x, 20x, and 40x air objectives was used to image the samples.

Optical clearing, confocal microscopy, and invasion assessment: Organoids were collected from the hanging drop plate and fixed as previously described. The paraformaldehyde was then aspirated and the organoids were rinsed three times with PBS containing azide (Santa Cruz) and stored at 4 °C for clearing. The organoids were rinsed consecutively in ethanol-PBS solutions containing increasing fractions of ethanol to dehydrate: 50%, 70%, 80%, 96%,

and two rinses at 100%, 3 minutes per rinse on a gently rocking platform. Then, the organoids were transferred to a chambered glass slide, and submerged in the clearing solution of benzyl alcohol/benzyl benzoate (BABB, 1:2 (v/v)). Imaging was conducted using a Perkin Elmer UltraView VoX spinning disc confocal microscope. Z-stacks were acquired with a 10x objective and 4.4 micron spacing. Confocal stacks were deconvolved using a calculated point spread function in Volocity Restoration software (Quorum Technologies) to better resolve relative cell positioning. The confocal stacks were analyzed in a double-blind manner; the images from the different timepoints were de-identified and then assessed for the presence of invasion by a different individual.

Statistical analysis: For quantification of morphological parameters, 20 organoids were used for each condition. The mean values are reported, and error bars represent the standard deviation. Multiple t-tests were performed to analyze the difference in area and roundness between organoid culture with and without Matrigel for days 2, 4, 7, 10, 13, and 16 of culture. * denotes a p-value <0.005 and ** denotes a p-value <0.000001. For invasion experiments, n = 8 organoids were used for the addition of MDA-MB-231 cells on day 7 and n = 5 organoids for their addition on day 16. Bar graphs were produced to show the percentage of organoids exhibiting invasion for each condition. All graphs were produced and statistical tests were performed using GraphPad Prism.

Supporting Information

Supporting Information is available from the Wiley Online Library or from the author.

Acknowledgements

This work was supported by NIH (R01CA196018, U01CA210152, and R50CA221807) and NSF EBICS (CBET-0939511). This material is also based upon work supported by the National Science Foundation Graduate Research Fellowship Program to EP (Grant Number: DGE-1650044). We also thank NSF ERC CMaT (EEC-1648035). All schematics included in the figures were produced with BioRender.

References

[1] M. E. Katt, A. L. Placone, A. D. Wong, Z. S. Xu, P. C. Searson, *Front. Bioeng. Biotechnol.* **2016**, *4*.

[2] P. Saglam-Metiner, S. Gulce-Iz, C. Biray-Avci, *Gene* **2019**, *686*, 203.

[3] Y. Fang, R. M. Eglen, *SLAS Discov.* **2017**, *22*, 456.

[4] N. Sachs, J. de Ligt, O. Kopper, E. Gogola, G. Bounova, F. Weeber, A. V. Balgobind, K. Wind, A. Gracanin, H. Begthel, J. Korving, R. van Boxtel, A. A. Duarte, D. Lelieveld, A. van Hoeck, R. F. Ernst, F. Blokzijl, I. J. Nijman, M. Hoogstraat, M. van de Ven, D. A. Egan, V. Zinzalla, J. Moll, S. F. Boj, E. E. Voest, L. Wessels, P. J. van Diest, S. Rottenberg, R. G. J. Vries, E. Cuppen, H. Clevers, *Cell* **2018**, *172*, 373.

[5] M. Huch, J. A. Knoblich, M. P. Lutolf, A. Martinez-Arias, *Dev.* **2017**, *144*, 938.

[6] J. Y. Co, M. Margalef-Català, X. Li, A. T. Mah, C. J. Kuo, D. M. Monack, M. R. Amieva, *Cell Rep.* **2019**, *26*, 2509.

[7] A. J. Ewald, R. J. Huebner, H. Palsdottir, J. K. Lee, M. J. Perez, D. M. Jorgens, A. N. Tauscher, K. J. Cheung, Z. Werb, M. Auer, *J. Cell Sci.* **2012**, *125*, 2638.

[8] J. Debnath, S. K. Muthuswamy, J. S. Brugge, *Methods* **2003**, *30*, 256.

[9] M. Sameni, D. Cavallo-Medved, O. E. Franco, A. Chalasani, K. Ji, N. Aggarwal, A. Anbalagan, X. Chen, R. R. Mattingly, S. W. Hayward, B. F. Sloane, *Breast Cancer Res.* **2017**, *19*, 1.

[10] S. I. Djomehri, B. Burman, M. E. Gonzalez, S. Takayama, C. G. Kleer, *J. Cell Commun. Signal.* **2019**, *13*, 129.

[11] M. Simian, M. J. Bissell, *J. Cell Biol.* **2017**, *216*, 31.

[12] S. Florian, Y. Iwamoto, M. Coughlin, R. Weissleder, T. J. Mitchison, *Proc. Natl. Acad. Sci. U. S. A.* **2019**, *166*, 11444.

[13] N. Akhtar, C. H. Streuli, *Nat. Cell Biol.* **2013**, *15*, 17.

[14] T. Gudjonsson, L. Rønnov-Jessen, R. Villadsen, F. Rank, M. J. Bissell, O. W. Petersen, *J. Cell Sci.* **2002**, *115*, 39.

[15] X. Wang, L. Suna, M. V. Maffinib, A. Sotob, C. Sonnenscheinb, D. L. Kaplan, *Biomaterials* **2010**, *31*, 3920.

[16] H. Wang, S. Lacoche, L. Huang, B. Xue, S. K. Muthuswamy, *Proc. Natl. Acad. Sci. U. S. A.* **2013**, *110*, 163.

[17] A. Gaiko-Shcherbak, G. Fabris, G. Dreissen, R. Merkel, B. Hoffmann, E. Noetzel, *PLoS One* **2015**, *10*, 1.

[18] T. R. Sarkar, S. Sharan, J. Wang, S. A. Pawar, C. A. Cantwell, P. F. Johnson, D. K. Morrison, J.-M. Wang, E. Sterneck, *Mol. Cell. Biol.* **2012**, *32*, 320.

[19] K. M. Imbalzano, I. Tatarkova, A. N. Imbalzano, J. A. Nickerson, *Cancer Cell Int.* **2009**, *9*, 1.

[20] A. Sonnenberg, J. Calafat, H. Janssen, H. Daams, L. M. H. Van Der Raaij-Helmer, R. Falconi, S. J. Kennel, J. D. Aplin, J. Baker, M. Loizidou, D. Garrod, *J. Cell Biol.* **1991**, *113*, 907.

[21] S. Yonemura, *PLoS One* **2014**, *9*, 1.

[22] S. Pawlizak, A. W. Fritsch, S. Grosser, D. Ahrens, T. Thalheim, S. Riedel, T. R. Kießling, L. Oswald, M. Zink, M. L. Manning, J. A. Käs, *New J. Phys.* **2015**, *17*.

[23] L. P. Ivers, B. Cummings, F. Owolabi, K. Welzel, R. Klinger, S. Saitoh, D. O'Connor, Y. Fujita, D. Scholz, N. Itasaki, *Cancer Cell Int.* **2014**, *14*.

[24] V. Espina, L. A. Liotta, *Nat. Rev. Cancer* **2011**, *11*, 68.

[25] K. L. Gorringe, S. B. Fox, *Front. Oncol.* **2017**, *7*.

[26] S. P. Carey, A. Starchenko, A. L. McGregor, C. A. Reinhart-King, *Clin. Exp. Metastasis* **2013**, *30*, 615.

[27] R. A. Foty, M. S. Steinberg, *Dev. Biol.* **2005**, *278*, 255.

[28] R. A. Foty, M. S. Steinberg, *Int. J. Dev. Biol.* **2004**, *48*, 397.

[29] S. Bartfeld, T. Bayram, M. Van De Wetering, M. Huch, H. Begthel, P. Kujala, R. Vries, P. J. Peters, H. Clevers, *Gastroenterology* **2015**, *148*, 126.

[30] E. J. Brock, K. Ji, S. Shah, R. R. Mattingly, B. F. Sloane, *J. Mammary Gland Biol. Neoplasia* **2019**, *24*, 1.

[31] L. L. Bischel, D. J. Beebe, K. E. Sung, *BMC Cancer* **2015**, *15*.

[32] K. E. Sung, N. Yang, C. Pehlke, P. J. Keely, K. W. Eliceiri, A. Friedl, D. J. Beebe, *Integr. Biol.* **2011**, *3*, 439.

[33] Y. Choi, E. Hyun, J. Seo, C. Blundell, H. C. Kim, E. Lee, S. H. Lee, A. Moon, W. K. Moon, D. Huh, *Lab Chip* **2015**, *15*, 3350.

[34] J. M. Ayuso, A. Gillette, K. Lugo-Cintrón, S. Acevedo-Acevedo, I. Gomez, M. Morgan, T. Heaster, K. B. Wisinski, S. P. Palecek, M. C. Skala, D. J. Beebe, *EBioMedicine* **2018**, *37*, 144.

[35] M. Sameni, A. Anbalagan, M. B. Olive, K. Moin, R. R. Mattingly, B. F. Sloane, *J. Vis. Exp.* **2012**, 1.

[36] S. A. Eccles, C. Box, W. Court, *Biotechnol. Annu. Rev.* **2005**, *11*, 391.

[37] D. L. Livant, S. Linn, S. Markwart, J. Sinister, *Cancer Res.* **1995**, *55*, 5085.

[38] P. Nowak-Sliwinska, T. Segura, M. L. Iruela-Arispe, *Angiogenesis* **2014**, *17*, 779.

[39] T. D. Russell, S. Jindal, S. Agunbiade, D. Gao, M. Troxell, V. F. Borges, P. Schedin, *Am. J. Pathol.* **2015**, *185*, 3076.

[40] P. R. Pandey, J. Saidou, K. Watabe, *Front Biosci.* **2010**, *15*, 226.

[41] S. Damiani, M. Ludvikova, G. Tomasic, S. Bianchi, A. M. Gown, V. Eusebi, *Virchows Arch.* **1999**, *434*, 227.

[42] M. P. V. Shekhar, L. Tait, R. J. Pauley, G. S. Wu, S. J. Santner, P. Nangia-Makker, V. Shekhar, H. Nassar, D. W. Visscher, G. H. Heppner, F. R. Miller, *Cancer Biol. Ther.* **2008**, *7*, 1774.

[43] Y. Shen, Y. Hou, S. Yao, P. Huang, L. Yobas, *Sci. Rep.* **2015**, *5*.

[44] A. Z. Wang, G. K. Ojakian, W. J. Nelson, *J. Cell Sci.* **1990**, *95*, 153.

[45] J. E. Wosen, A. Ilstad-Minnihan, J. Y. Co, W. Jiang, D. Mukhopadhyay, N. Q.

Fernandez-Becker, C. J. Kuo, M. R. Amieva, E. D. Mellins, *Front. Immunol.* **2019**, *10*, 1.

[46] J. W. Song, S. P. Cavnar, A. C. Walker, K. E. Luker, M. Gupta, Y. C. Tung, G. D. Luker, S. Takayama, *PLoS One* **2009**, *4*.

[47] Y. C. Tung, A. Y. Hsiao, S. G. Allen, Y. S. Torisawa, M. Ho, S. Takayama, *Analyst* **2011**, *136*, 473.

[48] B. M. Leung, S. C. Lesher-Perez, T. Matsuoka, C. Moraes, S. Takayama, *Biomater. Sci.* **2015**, *3*, 336.

[49] C. A. Schneider, W. S. Rasband, K. W. Eliceiri, *Nat. Methods* **2012**, *9*, 671.

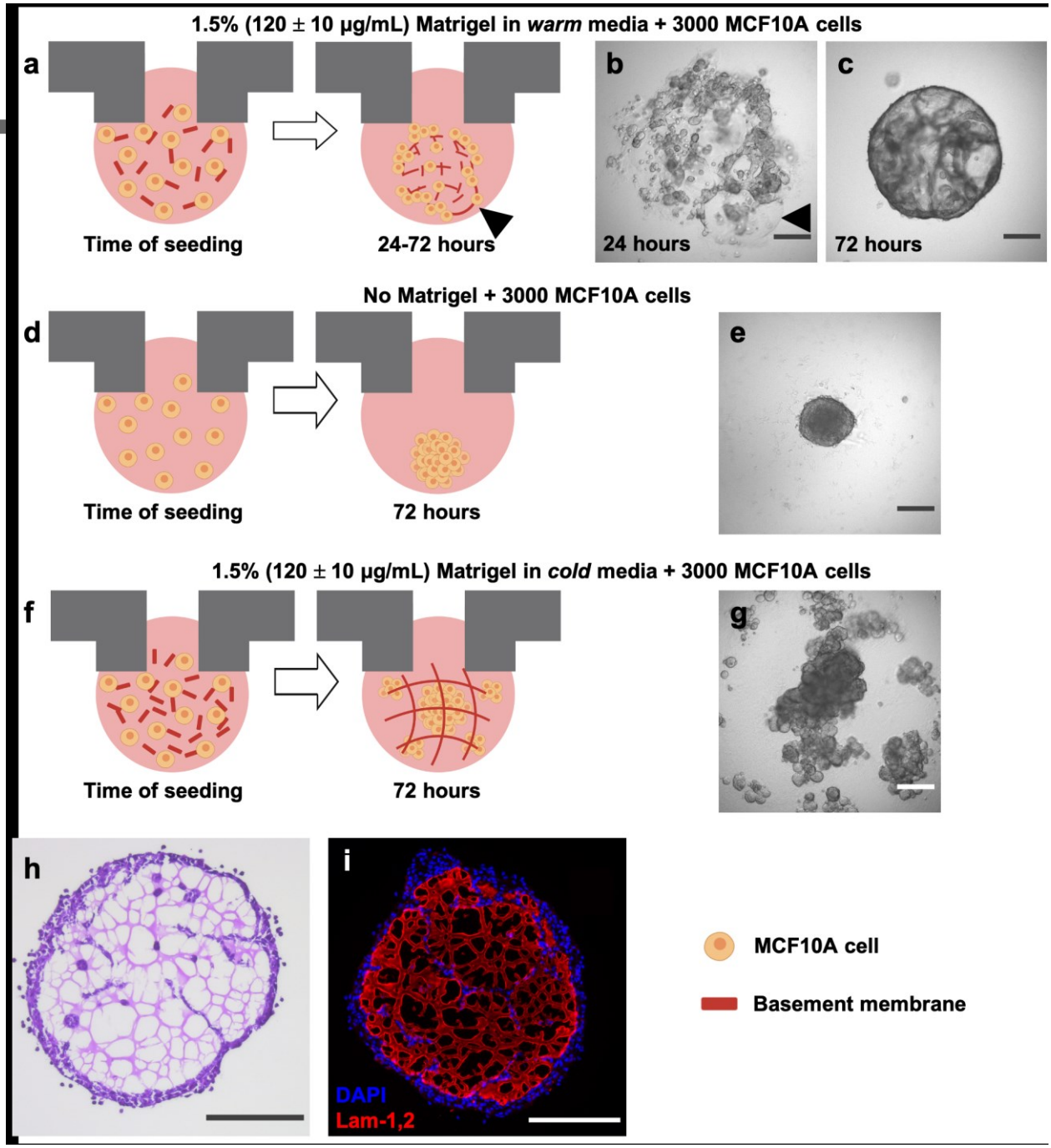

Figure 1. Cell-assisted minimal scaffolding is critical for organoid formation. Schematic representations (a, d, f) and brightfield images (b, c, e, g) of 1.5% Matrigel added to warm media, MCF10A cells with no Matrigel, and 1.5% (120 ± 10 µg/mL) Matrigel added to cold media, respectively. Black arrow in a and b shows a pocket of Matrigel. (h) H&E image of a day 16 organoid section. (i) Laminin-1,2 stain of a day 16 organoid section. All scale bars represent 200 µm.

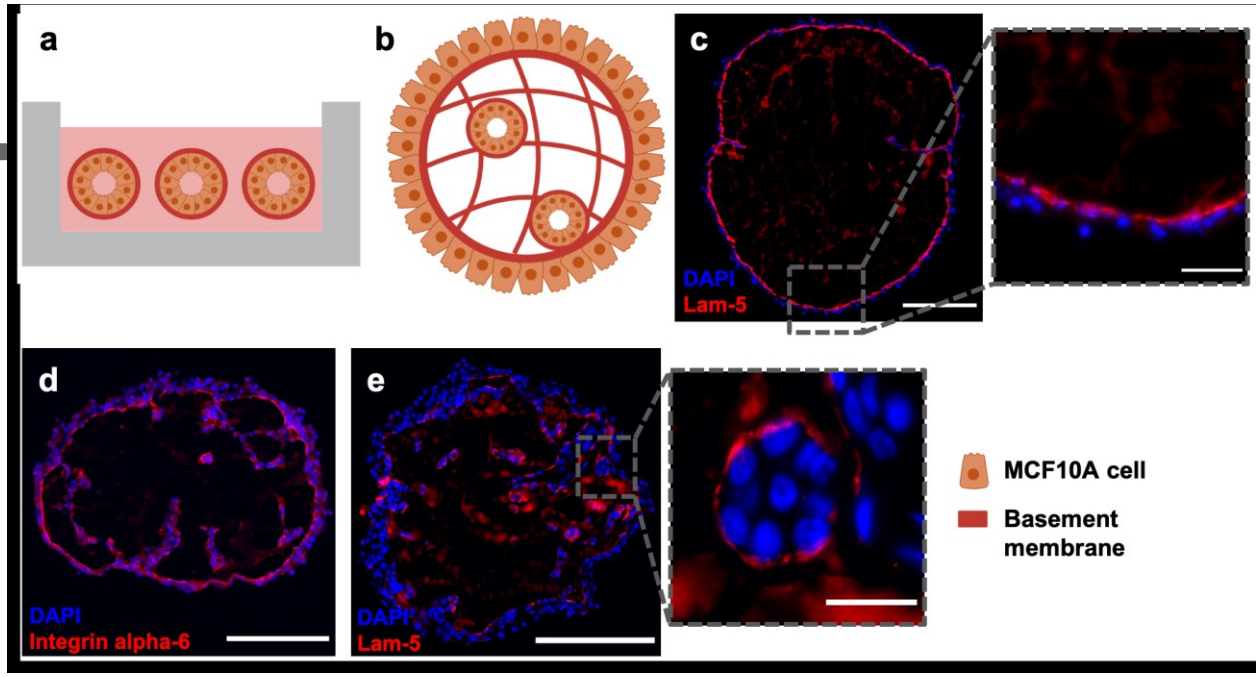

Figure 2. MCF10A organoids exhibit a basal-in phenotype. (a) Commonly observed, basal-out structure of MCF10A acini grown in gels. (b) Basal-in phenotype of MCF10A organoids described here. Smaller internal acinar structures maintain basal-out morphology. (c) Laminin-5 staining of a day 16 organoid section. Scale bar represents 200 μm. Inset shows 40x image, with laminin-5 layer on the inner side of the structure. Scale bar represents 50 μm. (d) Integrin alpha-6 staining of a day 16 organoid section. Scale bar represents 200 μm. (e) Laminin-5 staining of a day 12 organoid with a lesser extent of hollowing. Scale bar represents 200 μm. Inset shows 40x image of internal acinar-like structures that do not exhibit a basal-in morphology. Scale bar represents 20 μm.

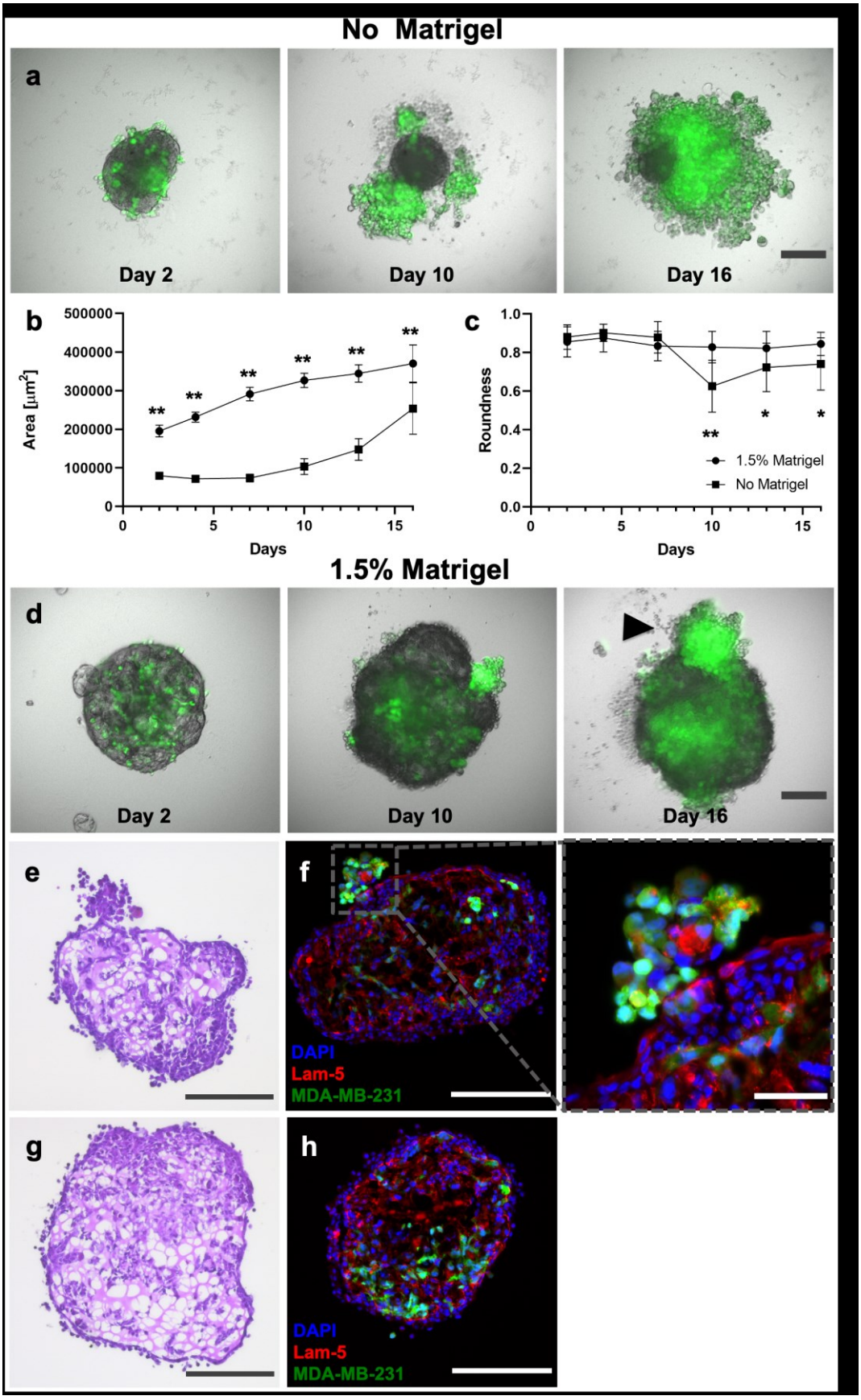

Figure 3. Self-organizing behaviors of MCF10A and MDA-MB-231 co-culture. (a) Time course development of co-culture without Matrigel. (b) Area and (c) roundness of co-culture both with and without Matrigel. The mean values are reported, and error bars represent the

standard deviation; n = 20 organoids were used for each condition. (d) Time course development of co-culture with 1.5% (120 ± 10 µg/mL) Matrigel. Black arrow in d indicates the peripheral ball of MDA-MB-231 cells. H&E image (e) and laminin-5 stain (f) of a day 16 co-culture organoid where a peripheral MDA-MB-231 ball remained attached to the main organoid body. H&E image (g) and laminin-5 stain (h) of a day 16 co-culture organoid where a peripheral ball of MDA-MB-231 cells dissociated from the organoid, which represents a majority of the co-culture organoids. All scale bars represent 200 µm, except the inset in (f) which represents 50 µm. * denotes a p-value <0.005 and ** denotes a p-value <0.000001.

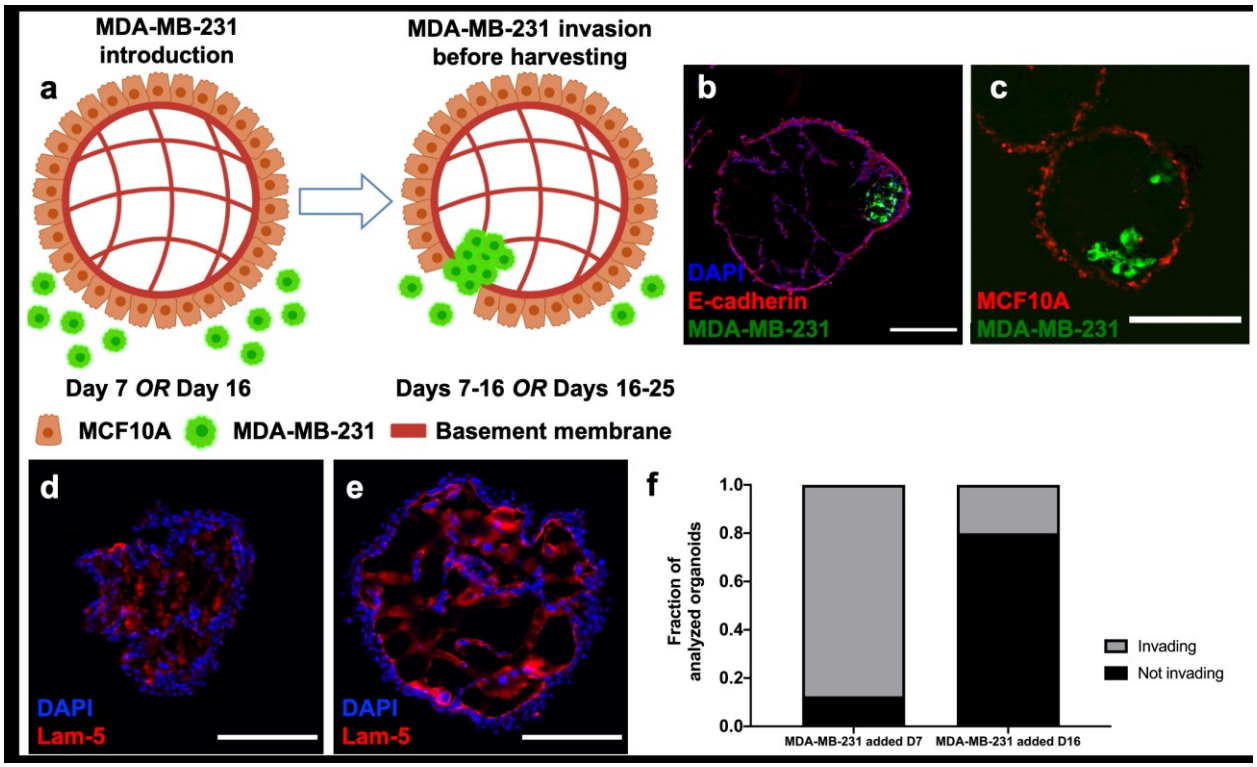

Figure 4. MCF10A organoid model as a cancer invasion platform. (a) Schematic of cancer invasion experiments. Organoids are grown to partial maturity, and MDA-MB-231 cancer cells are introduced on day 7 or 16. Due to the basal-in nature of the organoids, there is easy apical-surface access, represented by the outside of the organoid. Organoids were maintained in culture for an additional 9 days before fixation. (b) E-cadherin staining of MCF10A organoids after MDA-MB-231 cells invaded inside. Scale bar represents 200 µm. (c) Confocal slice at midplane of a cleared organoid showing MDA-MB-231 cancer invasion introduced at day 7 and maintained for 9 additional days. Scale bar represents 300 µm. (d) Laminin-5 staining of the basement membrane development over time at day 8 and (e) day 16. Scale bars represent 200 µm. (f) Quantification of percent of organoids showing cancer invasion when MDA-MB-231 cells were added on day 7 (n = 8) or day 16 (n = 5) of MCF10A organoid culture.

This paper describes the basal-in phenotype of organotypic structures formed from MCF10A cells, in which a cell-produced basement membrane is located on the interior side of the organoid. Because of the conveniently located apical surface, represented by the region exposed to the media surrounding the organoid, this platform shows promise as a high-throughput cancer invasion assay.